CONDENSED
MATTER
PHYSICS

An ab initio study of the static, dynamic and electronic properties of some liquid 5d transition metals near melting

D. J. González [iD] , L. E. González [iD]

Departamento de Física Teórica, Universidad de Valladolid, 47011 Valladolid, Spain

We report a study on the static and dynamic properties of several liquid $5d$ transition metals at thermodynamic conditions near their respective melting points. This is performed by resorting to *ab initio* molecular dynamics simulations in the framework of the density functional theory. Results are presented for the static structure factors and pair distribution functions; moreover, the local short range order in the liquid metal is also analized. As for the dynamical properties, both single-particle and collective properties are evaluated. The dynamical structure shows the propagating density fluctuations, and the respective dispersion relation is obtained. Results are also obtained for the longitudinal and transverse current spectral functions along with the associated dispersion of collective excitations. For some metals, we found the existence of two branches of transverse collective excitations in the region around the main peak of the structure factor. Finally, several transport coefficients are also calculated.

Key words: *liquid metals, transition metals, first principles calculations*

1. Introduction

This paper reports an *ab initio* molecular dynamics (AIMD) simulation study on the static, dynamic and electronic properties of several liquid $5d$ transition metals (Hf, Ta, W, Re, Os, Ir, Pt and Au) at thermodynamic conditions just above melting at room pressure.

Except Au, all the other metals belong to the group of the so-called refractory metals which are characterized by very high melting points ($\geqslant 2000$ K). They also share some properties such as high density, retention of mechanical strength at high temperatures, high hardness at room temperature and resistance to the damages of corrosion, wear and deformation. Because of their exceptional high-temperature properties, the refractory metals and alloys are a good choice for high-temperature applications, e. g., those materials used for fission and fusion reactors (first wall, blanket and divertor).

Other interesting applications of these metals have to do with defense and aerospace industries, medical devices, low-temperature superconductor applications, manufacture of very hard-wearing and durable electrical components, chemical industry, etc. Consequently, all those above mentioned technological applications justify the research effort aimed at achieving a better understanding of their structural, dynamical and electronic properties.

In this paper we are focused on the molten state, which because of the high melting temperatures and high reactivity of these refractory metals, poses important challenges when trying to measure their liquid state properties. Nevertheless, a good understanding of their thermophysical properties is important for the studies on phase transformations, nucleation, atomic dynamics and surface physics as well as industrial processes (i.e., refining, casting and welding) and for designing alloys.

Notwithstanding the technological relevance of these metals, there is a scarcity of experimental data concerning their static, dynamic and electronic properties in the molten state; obviously, this is related to the challenges posed by their high melting temperatures.

Two basic magnitudes related to the structural short-range order in a liquid metal are the static structure factor, $S(q)$, and the pair distribution function, $g(r)$. In the case of the liquid $5d$ metals considered in this work, it is no wonder that the available experimental structural data are for the two metals with the lowest melting temperature, namely, Pt and Au. In fact, these data were obtained, more than forty years ago, by Waseda and coworkers [1] that performed X-ray diffraction (XD) measurements of the $S(q)$ of liquid l-Pt and l-Au at thermodynamic conditions near their respective melting points. Since then, no additional measurements of the $S(q)$ have been performed for any of these liquid metals with the exception of l-Ta for which XD experiments have been recently performed under thermodynamic conditions of internal negative pressure [2] and results have been obtained for its $S(q)$ in a pressure range from 5.6 GPa to 2.7 GPa.

As for the dynamical properties, we mention the experimental study by Guarini et al. [3] on the microscopic dynamics of l-Au at $T = 1373$ K. Specifically, they performed inelastic neutron scattering (INS) measurements, and the dynamic structure factor, $S(q, \omega)$, was determined within the range $0.6 \leqslant q \leqslant 1.6$ Å^{-1}. The propagating collective excitations were detected and its associated dispersion relation yielded an adiabatic velocity of sound in good agreement with the experimental value of ≈ 2568 m/s [4]. We are not aware of any similar study performed for any of the other $5d$ metals considered in this work. In the same study, the authors also performed AIMD simulations that showed good agreement with the experimental data.

The additional available experimental data refer to the transport coefficients only. The sound velocity was measured, in addition to l-Au, for l-Ta, l-W and l-Pt [4]. The shear viscosities were measured by Ishikawa et al. [5–8] by means of levitation techniques; however, their diffusion coefficients have not been determined yet.

This shortage of experimental data for this group of metals highlights the importance of resorting to other approaches such as theoretical and computer simulation methods to extract information about their static, dynamic and electronic properties.

However, few theoretical studies, either based on semiempirical or more fundamental methods, have been devoted to the study of these liquid $5d$ transition metals so far and they have mainly focused on thermodynamic and static structural properties. There are a few studies based on the effective potentials for l-Pt and l-Au, by Alemany et al. [9, 10] and by Gosh et al. [11], where the static structure and some transport properties were evaluated. Using a more fundamental approach Bhuiyan et al. [12] performed a MD study of several static and dynamic properties of l-Au near melting by resorting to the orbital-free ab initio MD simulation method (OF-AIMD), which is based on the Hohenberg and Kohn version [13] of the Density Functional Theory (OF-DFT), where the basic variable is the total valence electronic density. They obtained good results for the static structure as well as for some transport coefficients such as the diffusion coefficient and the shear viscosity. In addition to those already mentioned for l-Au [3], we finally mention AIMD simulations based on the Kohn-Sham formulation of DFT (KS-DFT) [14] that were performed for l-Ta and undercooled l-Ta by Jakse et al. [15, 16], where the static structure was studied, and those for l-Pt by del Rio et al. [17] that evaluated several transport properties and static and dynamic structural properties, reporting good agreement with experiments. Some of those results for l-Pt are included in this work for completion.

The AIMD simulation study presented in this paper, is based on the KS-DFT formalism. The liquid metal is modelled as an interacting system of ions and electrons and for any ionic configuration, the associated electronic ground state is evaluated by means of the KS-DFT approach. Then, the forces acting on the ions are obtained via the Hellmann-Feynman theorem, and their positions evolve according to classical mechanics while the electronic subsystem follows adiabatically. The present AIMD simulation method requires large computational capabilities and imposes severe limitations concerning the simulation times and size of the systems under study; however, these disadvantages are somewhat balanced by the accuracy of the obtained results.

The paper is structured as follows: the next section summarizes the basic ideas underlying the AIMD simulation method along with some technical details. In section 3 we report the results of the calculations which are compared with the available experimental data along with some discussion. Finally, a brief summary and conclusions are given in section 4.

2. Computational method

Table 1 lists the specific $5d$ metals and the corresponding thermodynamic states for which the AIMD simulation study is performed. The simulations were carried out by using a cubic cell containing 120 atoms (150 atoms in l-Au).

The AIMD simulations were implemented using the DFT based Quantum-ESPRESSO package [18, 19]. Within this framework, the electronic exchange-correlation energy was described by the generalized gradient approximation of Perdew-Burke-Ernzerhof [20], except l-Pt and l-Au for which we used the local density approximation of Perdew and Zunger [21]. On the other hand, the ion-electron interaction was accounted for by means of an ultrasoft pseudopotential [22], which was generated from a scalar-relativistic calculation and it included non-linear core corrections. The only exception was l-Ir for which we used a norm-conserving Troulliers-Martins type pseudopotential. Table 1 specifies, for each metal, the number of valence electrons which are explicitly considered in the calculation. Note that in the cases of Hf through Os the $5s$ and $5p$ electrons are included as semi-core states.

The simulations started with the ions placed at some random initial positions within the cell and then the system was thermalized during $5 - 10$ ps of simulation time; therefrom, microcanonical AIMD simulations, with a time step of 0.0055 ps (0.0075 ps for l-Au), were performed over the number of time steps given in table 1. We used a plane-wave representation with an energy cutoff within the range from 25 to 40 Ry for the wavefunctions and 150 to 350 Ry for the electronic density. The single Γ point was used for sampling the Brillouin zone.

The number of equilibrium configurations listed in table 1 were those used for the evaluation of the static, dynamic and electronic properties of the corresponding liquid metal. We notice that this same simulation method has already proved its capability to deliver an accurate description of several static, dynamic and transport properties of other bulk liquid metals [23–32].

Table 1. Thermodynamic input data of the liquid $5d$ transition metals considered in the present AIMD simulation study, where ρ is the total ionic number density (taken from [5]), T is the temperature, N_{part} is the number of particles in the simulation box, Z_{val} is the number of valence electrons in the pseudopotential and N_c is the total number of generated configurations.

	ρ (Å^{-3})	T(K)	N_{part}	Z_{val}	N_c
Hf	0.0382	2550	120	12	12000
Ta	0.0473	3350	120	13	13000
W	0.0562	3750	120	14	13000
Re	0.0591	3600	120	15	10500
Os	0.0605	3400	120	16	11500
Ir	0.0623	2750	120	9	20000
Pt	0.0577	2053	120	10	19500
Au	0.0526	1423	150	11	20000

3. Results and discussion

3.1. Static properties

The results obtained for the respective static structure factors, $S(q)$, are plotted in figures 1–2, where they are compared with the (scarce) available experimental data. We observe that for both l-Pt and l-Au there is a very good agreement, both in the position and amplitude of the oscillations, with the corresponding XD data. As for the other $5d$ liquid metals considered in this study, there are no structural data available for comparison. In the case of l-Ta, the recent XD measurements refer to thermodynamic states different from the present AIMD simulations.
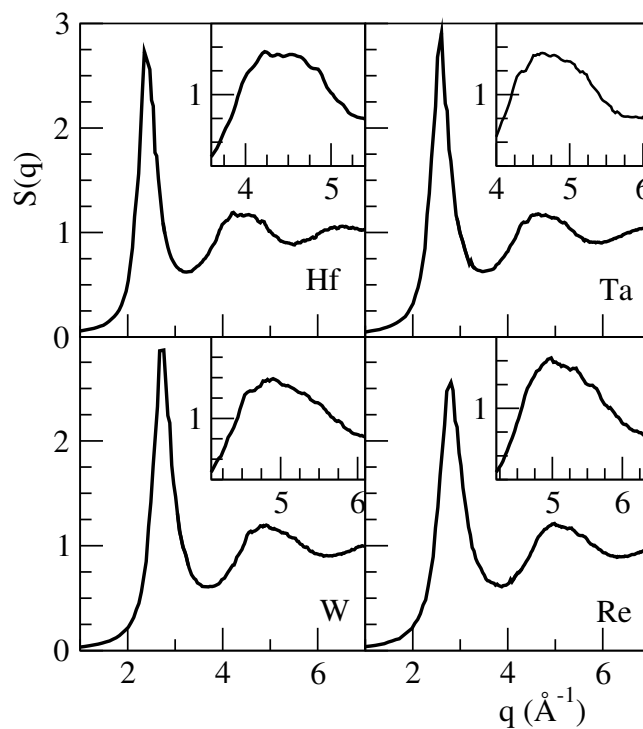
Figure 1. Static structure factor, $S(q)$, of l-Hf, l-Ta, l-W and l-Re. Continuous line: present AIMD calculations. The inset shows a closer view of the second maximum.
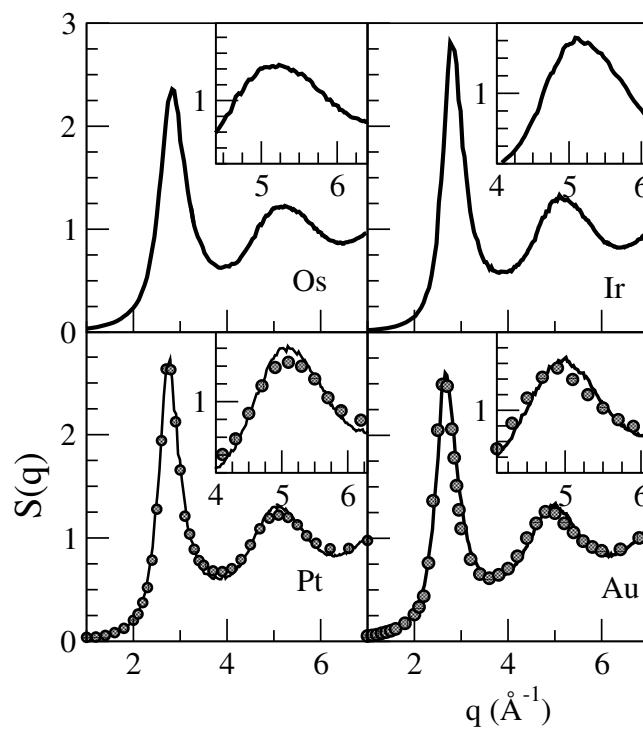

Figure 2. Same as the previous graph but for l-Os, l-Ir, l-Pt [17] and l-Au. Symbols: XD data from Waseda's group [1, 33].

Figures 1–2 also provide a closer look at the shape of the second peak of the $S(q)$. We obtain a noticeable asymmetric shape in the group from l-Hf to l-Re but it becomes more symmetric for l-Os, l-Ir and l-Au. We mention that an asymmetric shape of the second peak with a shoulder on its high-q side was experimentally found in several liquid metals, including some transition metals (Ti, Fe, Ni) [34–36] and it was interpreted as an indicator of a noticeable existence of icosahedral local order in the liquid.

We used the low-q values of the calculated $S(q)$, i.e., the values within the range $q \leqslant 1.2\,\text{Å}^{-1}$, to obtain a rough estimate for $S(q \to 0)$. This is achieved by using a least squares fitting of $S(q) = s_0 + s_2 q^2$, and the results are given in table 2. Then, the relation where k_B is Boltzmann's constant, allows to determine the associated isothermal compressibility, κ_T, and the results are given in table 2. We additionally included the values suggested by Marcus [37], which were obtained by using semiempirical expressions which involve the measured and/or estimated values of several other thermophysical magnitudes, and also the experimental values reported by Blairs [4] for l-Ta, l-W, l-Pt and l-Au.

Table 2. The calculated values for $r_{\min}$ (in Å), coordination numbers CN, $S(q \to 0)$ and isothermal compressibilities κ_T (in $10^{-11}\,\text{Pa}^{-1}$ units) for the liquid $5d$ transition metals at the thermodynamic states given in table 1. The results for l-Pt are taken from [17]. The numbers in parenthesis are semiempirical estimates from Marcus [37]. Experimental data for κ_T at the melting temperature are taken from [4].

	$r_{\min}$	CN	$S(q \to 0)$	κ_T	$\kappa_T^{\exp}$
Hf	4.23	12.2	0.024 ± 0.002	1.78 ± 0.20 (1.78)	
Ta	3.95	12.2	0.022 ± 0.002	1.01 ± 0.15 (1.68)	1.00
W	3.78	12.9	0.016 ± 0.002	0.55 ± 0.10 (0.99)	0.95
Re	3.62	12.1	0.015 ± 0.001	0.51 ± 0.05 (0.92)	
Os	3.51	11.3	0.014 ± 0.001	0.49 ± 0.05 (0.86)	
Ir	3.50	11.8	0.009 ± 0.001	0.36 ± 0.05 (0.82)	
Pt	3.77	12.8	0.011 ± 0.001	0.67 ± 0.05 (1.02)	0.84
Au	3.63	11.2	0.012 ± 0.001	1.09 ± 0.05 (1.19)	1.31

The pair distribution function, $g(r)$, provides some insight into the short range order in the liquid metal and figures 3-4 depict the obtained AIMD results along with the available experimental data. As it happened with the $S(q)$, we observe a very good agreement for both l-Pt and l-Au. The average number of nearest neighbors (also called coordination number, CN) around any given ion can be evaluated by integrating the radial distribution function, $4\pi \rho r^2 g(r)$, up to the position of its first minimum, $r_{\min}$. Table 2 lists the obtained results which are similar to those calculated for other simple liquid metals near melting [38].

A more thorough description of the short range order in a liquid metal is provided by the common neighbor analysis [39–41] (CNA) method. It gives three-dimensional information about the ions surrounding each pair of ions which are near neighbors. Each pair is characterized by four indices which allow to discern among different local structures like fcc, hcp, bcc, and icosahedral environments. Thus, the fcc order only has 1421-type pairs, the hcp structure has the same number of 1421 and 1422-type pairs, the bcc order has six 1441-types pairs and eight 1661 type-pairs and the 13-atom icosahedron (ico) has twelve 1551 type-pairs. The deformation of the regular 1551-type structure (i.e., when a bond is broken) yields the 1541 and 1431-type pairs and therefore their presence points to the existence of a somewhat distorted icosahedral order. Finally the 1311 and 1321-type pairs are related to disorderly structures. For more details about the CNA method we refer to references [30, 32, 39–41]. Table 3 and figure 5 summarize the results obtained in this work. The five-fold symmetry dominates in all these metals because the sum of perfect and distorted ico-structures ranges between $\approx 50\%$ (l-Au) and $\approx 72\%$ (l-Hf, l-Ta) of the pairs. The amount of local bcc-type pairs is significant in l-Hf, l-Ta and l-W whereas it is small for the other metals which, on the other hand, show an important amount of fcc and hcp-type pairs (from $\approx 12\%$ in l-Pt to $\approx 21\%$ in l-Au). Moreover, this group of metals also shows a noticeable fraction of disordered 13xx(1311 + 1321)-type pairs (from $\approx 8\%$ in l-Ir to $\approx 18\%$ in l-Au).

Our results for l-Ta are statistically equivalent to the early ones obtained by Jakse et al. in 2004 [15, 16] above the melting temperature. We do not discern hints of the A15 structure that they observed
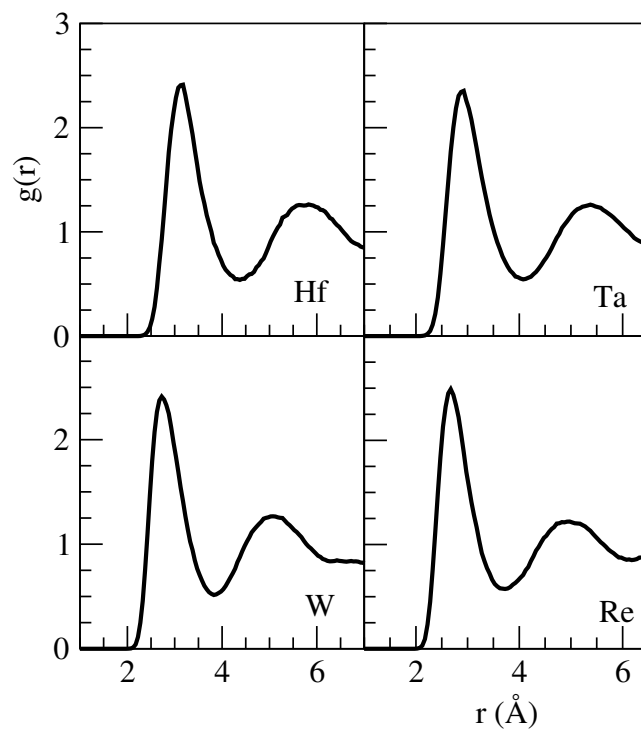
Figure 3. Pair distribution function, $g(r)$, of l-Hf, l-Ta, l-W and l-Re. Continuous line: present AIMD calculations.
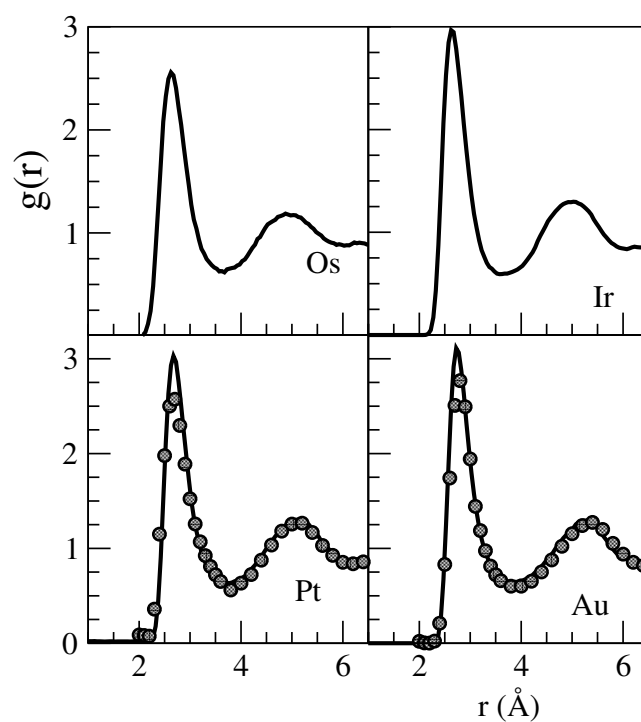

Figure 4. Same as the previous graph but for l-Os, l-Ir, l-Pt and l-Au. Symbols: XD data from Waseda's group [1, 33].

Table 3. Common neighbour analysis of the AIMD configurations obtained for the liquid $5d$ transition metals at the thermodynamic states given in table 1. For comparison we include the values for some common local structures. The data for l-Pt are taken from [17].

| Pairs	1551	1541	1431	1421	1422	1311	1321	1441	1661
l-Hf	0.28	0.21	0.22	0.04	0.05	0.02	0.03	0.08	0.10
l-Ta	0.32	0.19	0.21	0.02	0.05	0.02	0.03	0.06	0.09
l-W	0.30	0.19	0.19	0.02	0.03	0.02	0.03	0.06	0.09
l-Re	0.18	0.19	0.24	0.06	0.10	0.06	0.04	0.03	0.04
l-Os	0.17	0.18	0.23	0.05	0.09	0.09	0.07	0.03	0.04
l-Ir	0.17	0.22	0.23	0.06	0.09	0.04	0.04	0.04	0.05
l-Pt	0.14	0.21	0.22	0.07	0.10	0.06	0.05	0.05	0.04
l-Au	0.10	0.17	0.23	0.07	0.14	0.12	0.06	0.03	0.03
HCP	0.0	0.0	0.0	0.50	0.50	0.0	0.0	0.0	0.0
FCC	0.0	0.0	0.0	1.0	0.0	0.0	0.0	0.0	0.0
BCC	0.0	0.0	0.0	0.0	0.0	0.0	0.0	0.43	0.57
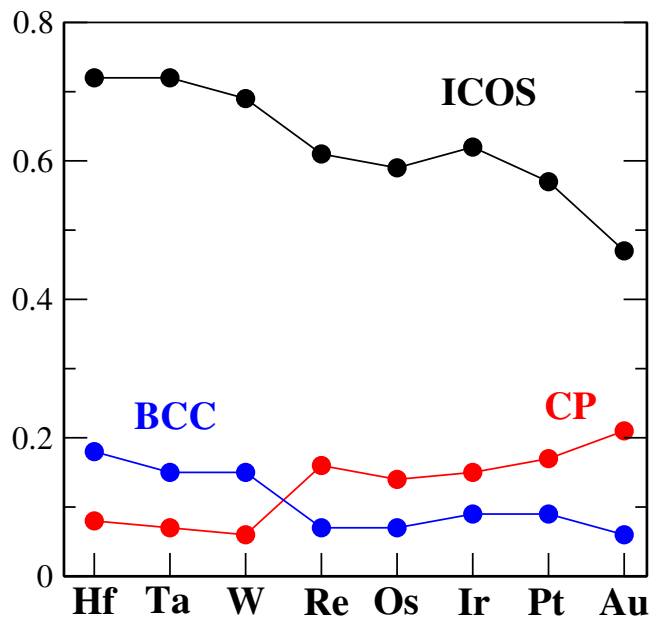
Figure 5. (Colour online) Variation of the most abundant bonded pairs.

in the undercooled liquid, because the ratio 1661 to 1441 is very similar to the one corresponding to bcc structures. Nevertheless, this signature was very dependent on the density of the undercooled liquid, so it is not surprising that it is absent in our liquid sample. It is also worth mentioning that the secondary structures present in the liquid $5d$ metals correlate well with the phases from which the corresponding solids melt, namely, bcc in the cases of Hf, Ta and W, and close-packed in the rest of cases (hcp for Re and Os, fcc for Ir, Pt and Au).

3.2. Dynamic properties

We have evaluated several dynamical properties obtained from time dependent correlation functions. Some of these functions depend on the wave-vector $\mathbf{q}$, but the isotropic behavior of the fluid allows to reduce such dependence to a dependence on $q \equiv |\mathbf{q}|$ only.

3.2.1. Single particle dynamics

The (normalized) velocity autocorrelation function (VACF) of a tagged ion in the fluid, $Z(t)$, is defined as

$$Z(t) = \langle \mathbf{v}_i(t) \cdot \mathbf{v}_i(0) \rangle / \langle v_i^2 \rangle, \tag{3.1}$$

with $\mathbf{v}_i(t)$ being the velocity of ion i at time t, and the angular brackets denote an average over particles and time origins.

Figures 6–7 show the obtained AIMD results for $Z(t)$. They display the typical decaying behavior with a marked first minimum related to the rebounding of the tagged atom against the cage formed by its near neighbors, followed by relatively weak oscillations that damp towards zero at longer times. Notice that the number density plays an important role in the single-particle dynamics: a higher density leads to a faster cage effect when moving from Hf to Ir, and a subsequent decrease in the density when moving towards Au produces some slowing down of the backscattering minimum.

The Fourier Transform (FT) of the $Z(t)$ into the frequency domain gives the associated power spectra, $Z(\omega)$ and these are plotted as insets in figures 6–7. Notice that the shapes of the $Z(\omega)$ may display just a peak (l-Hf) or a peak followed by a more/less marked shoulder located at a higher frequency. Similar qualitative results were obtained in previous AIMD studies of several $3d$ and $4d$ liquid metals [30–32]. Some authors [3, 42] have recently suggested the existence of a relation between the shape of the $Z(\omega)$ and the appearance of a special type of collective excitations. We will further comment about this point in the following section where we discuss our obtained results in connection with the transverse currents.

The self-diffusion coefficient, D, was calculated by both the time integral of $Z(t)$ and from the slope of the mean square displacement of a tagged ion in the fluid; both routes lead to practically the same results, which are given in table 4. We are not aware of any experimental self-diffusion data for the $5d$ metals considered in this work. Nevertheless, we included in table 4 some estimates obtained from semiempirical expressions based on the modified Stokes-Einstein type formulae which relate the self-diffusion coefficient to other thermophysical magnitudes such as density and viscosity [5].
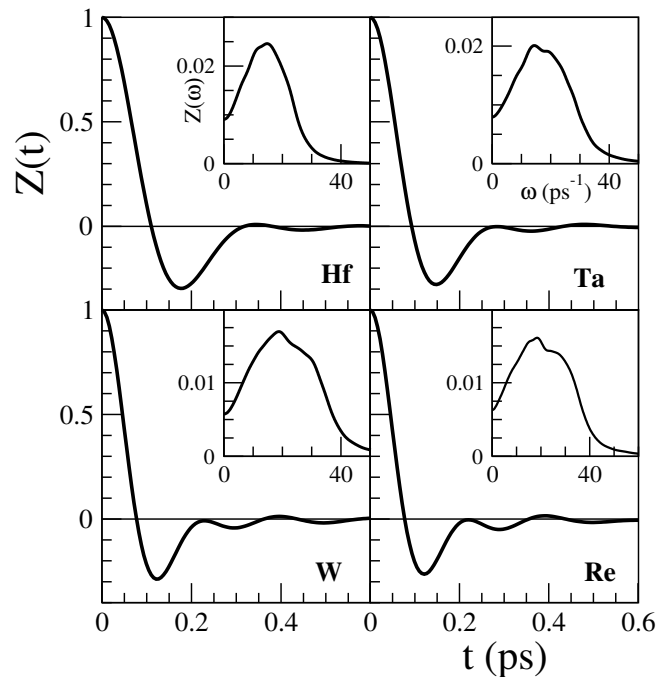

Figure 6. Normalized AIMD calculated velocity autocorrelation function of l-Hf, l-Ta, l-W and l-Re. The inset represents the corresponding power spectrum $Z(\omega)$.
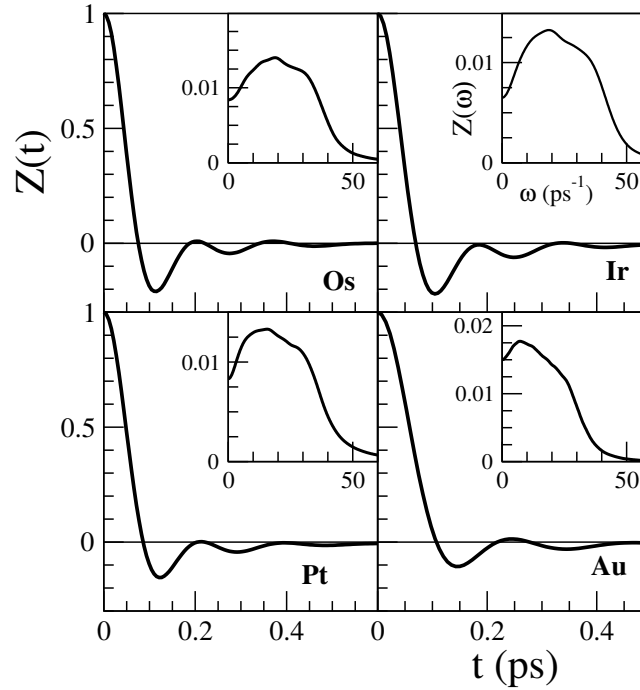
Figure 7. Same as the previous graph, but for l-Os, l-Ir, l-Pt [17] and l-Au.

3.2.2. Collective dynamics

The collective dynamics of density fluctuations in a liquid can be described by the intermediate scattering function, $F(\mathbf{q}, t)$, defined as

$$F(\mathbf{q}, t) = \frac{1}{N} \left\langle \sum_{i,j=1}^{N} \exp\left[i\, \mathbf{q} \cdot (\mathbf{R}_i(t) - \mathbf{R}_j(t=0))\right] \right\rangle, \tag{3.2}$$

whose time FT gives its frequency spectrum, known as the dynamic structure factor, $S(\mathbf{q}, \omega)$, which can be directly measured by either inelastic neutron scattering (INS) or inelastic X-ray (IXS) experiments.
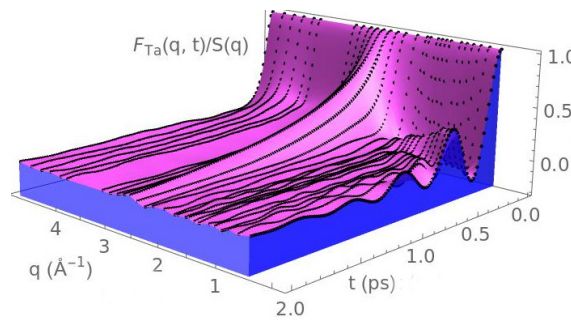

Figure 8. (Colour online) Intermediate scattering function, $F(q, t)/S(q)$, of l-Ta at $T = 3350$ K for several q values.

Figures 8–9 depict, for l-Ta and l-Au, the corresponding AIMD results for $F(q, t)$. The trends observed for these two metals are qualitatively similar for all the other metals: at small q's, there is an oscillatory behavior that subsides with increasing q-values and it has practically disappeared when $q \approx (4/5)\,q_p$, where q_p denotes the position of the main peak of $S(q)$. Then, for greater q values ($q > q_p$), the $F(q, t)$ exhibit a monotonously decaying shape. The associated $S(q, \omega)$ are plotted in figures 10–11, and

Table 4. The calculated values of the self-diffusion coefficient (D), adiabatic sound velocity (c_s) and shear viscosity (η) for the liquid $5d$ transition metals at the thermodynamic states given in table 1. The sound velocities included in the second lines for l-Ta, l-W, l-Pt and l-Au correspond to experimental values, and the second and third lines for the other elements are different semiempirical estimations. The viscosities reported in the second and third lines for each element are the measured values in different experiments.

|	D (Å^2/ps)	c_s (m/s)	η (GPa ps)
Hf	0.332 ± 0.020	2380 ± 150	4.90 ± 0.25
	0.418 [5]	2631, 2559 [4]	5.2 [6]
		3371 [5]	
Ta	0.378 ± 0.025	3180 ± 150	6.00 ± 0.30
	0.365[5]	3303 [4, 5]	8.6 [5]
			8.8 ± 0.9 [8]
W	0.307 ± 0.015	3890 ± 150	8.60 ± 0.40
	0.530[5]	3279 [4, 5]	7.0 [5]
			8.5 ± 0.9 [8]
Re	0.333 ± 0.020	3640 ± 150	7.60 ± 0.35
	0.447[5]	3569 [5]	7.9 [5]
		2943, 2665 [4]	9.9 ± 1.0 [8]
Os	0.395 ± 0.025	2860 ± 200	5.90 ± 0.30
	0.420[5]	3335 [5]	4.2 [5]
		2777, 2487 [4]	7.0 ± 0.7 [8]
Ir	0.227 ± 0.015	3620 ± 200	8.80 ± 0.40
	0.400[5]	3230 [5]	6.0, 7.0 [7]
		2643, 2416 [4]	
Pt	0.270 ± 0.015	3310 ± 200	4.90 ± 0.25
	0.305, 0.426[5]	3053 [4, 5]	4.82, 6.74 [5, 7]
Au	0.282 ± 0.015	2380 ± 200	3.50 ± 0.20
	0.243[5]	2568 [4, 5]	5.37 [5]
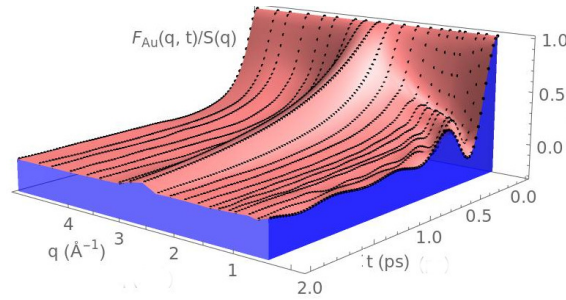
Figure 9. (Colour online) Intermediate scattering function, $F(q,t)/S(q)$, of l-Au at $T = 1423$ K for several q values.

show, up to $q \approx (3/5)\, q_p$, side-peaks which attest to the existence of collective density excitations; for greater q-values, the $S(q, \omega)$ display a monotonously decreasing behavior. This same qualitative trend is exhibited by all the other $5d$ metals considered in this paper.

For each metal, we determined the frequency of the side-peaks as a function of the wavevector, namely the function $\omega_m(q)$ which represents the associated dispersion relation of the density excitations and those are depicted in figures 12–13. The corresponding phase velocities are defined as $c_m(q) = \omega_m(q)/q$. These are plotted in figures 14–15 in the region $q \leqslant 1.2$ Å^{-1}. In the long wavelength limit ($q \to 0$), the phase velocity tends towards the adiabatic speed of sound, c_s. The extrapolation of the AIMD data to $q = 0$ is subject to some uncertainty because the minimum wavevector is restricted by the relatively
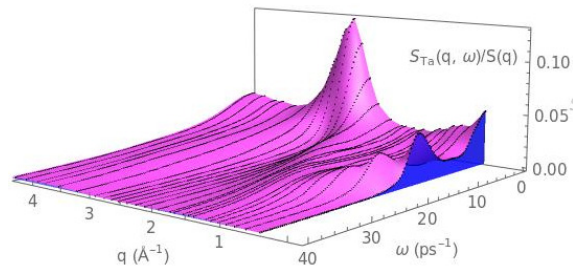
Figure 10. (Colour online) Dynamic structure factors, $S(q, \omega)/S(q)$, of l-Ta at $T = 3350$ K and several q values.
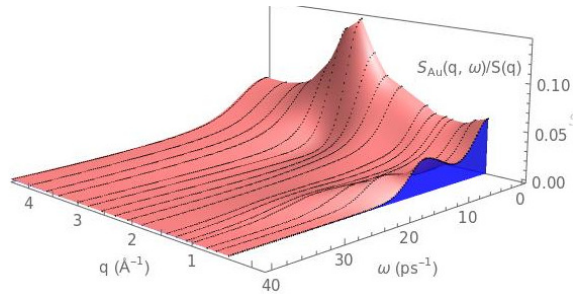

Figure 11. (Colour online) Dynamic structure factors, $S(q, \omega)/S(q)$, of l-Au at $T = 1423$ K and several q values.

small simulation box associated to the small number of particles affordable within the AIMD method. Nevertheless, there are some constraints that must be fulfilled in the long wavelength limit that we have implemented, and are related to the phase velocities associated to the longitudinal currents, which we define next.

The current due to the overall motion of the particles,

$$\mathbf{j}(\mathbf{q}, t) = \sum_{j=1}^{N} \mathbf{v}_j(t) \, \exp[\mathrm{i}\mathbf{q} \cdot \mathbf{R}_j(t)], \tag{3.3}$$

is usually split into a longitudinal component $\mathbf{j}_l(\mathbf{q}, t) = (\mathbf{j}(\mathbf{q}, t) \cdot \mathbf{q})\mathbf{q}/q^2$, and a transverse component $\mathbf{j}_t(\mathbf{q}, t) = \mathbf{j}(\mathbf{q}, t) - \mathbf{j}_l(\mathbf{q}, t)$. The longitudinal and transverse current correlation functions are obtained as

$$C_L(\mathbf{q}, t) = \frac{1}{N} \langle \mathbf{j}_l(\mathbf{q}, t) \cdot \mathbf{j}_l^*(\mathbf{q}, t = 0) \rangle \tag{3.4}$$

and

$$C_T(\mathbf{q}, t) = \frac{1}{2N} \langle \mathbf{j}_t(\mathbf{q}, t) \cdot \mathbf{j}_t^*(\mathbf{q}, t = 0) \rangle. \tag{3.5}$$

The respective time Fourier Transforms (FT) give the associated spectra $C_L(\mathbf{q}, \omega)$ and $C_T(\mathbf{q}, \omega)$.

For any fixed q-value, when the $C_L(q, \omega)$ is plotted as a function of ω we observe a maximum, and its associatted frequency, namely $\omega_L(q)$, stands for the dispersion relation of the longitudinal modes. These are plotted in figures 12–13 where it is observed that their shape shows a trend similar to that already observed in other liquid metals [43]. The associated phase velocities, $c_L(q) = \omega_L(q)/q$, are also plotted in figures 14–15, and must tend towards the same value, c_s, as the $c_m(q)$ when $q \to 0$. We performed a quadratic fit $c(q) = c_s + aq + bq^2$ to the phase velocities $c_m(q)$ and $c_L(q)$ in the q range shown in figures 14–15 imposing a common value c_s at $q = 0$. In all cases we obtain a positive value of the coefficient a, an effect named as positive dispersion that is quite usual in liquid metals near their melting points at ambient pressure, and was rationalized by Bryk and coworkers resorting to theoretical models based on the generalized collective modes approach [44]. The results obtained for c_s are given

in table 4, which also includes for comparison the available experimental (l-Ta, l-W, l-Pt, l-Au) [4] and semiempirical (l-Hf, l-Re, l-Os, l-Ir) [4, 5] data. These latter data are the estimates obtained from some semiempirical formulae [4] which relate the adiabatic sound velocity to other thermophysical magnitudes such as surface tension, density and melting temperature. Overall, we observe a good agreement between the AIMD results and the experimental/semiempirical data, with the greatest discrepancies observed for l-W and l-Ir.
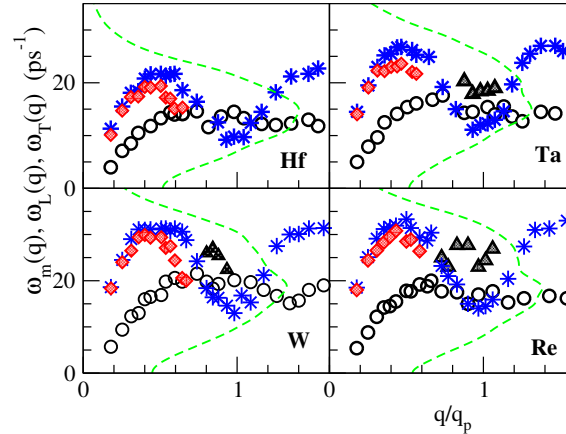
Figure 12. (Colour online) Dispersion relations for l-Hf, l-Ta, l-W and l-Re. Red diamonds and blue stars: longitudinal dispersion obtained from the AIMD results for the positions of the inelastic peaks in the $S(q, \omega)$ and from the maxima in the spectra of the longitudinal current, $C_L(q, \omega)$, respectively. Open circles and triangles: transverse dispersion from the positions of the peaks in the spectra $C_T(q, \omega)$. The green dashed line represents the corresponding $Z(\omega)$.
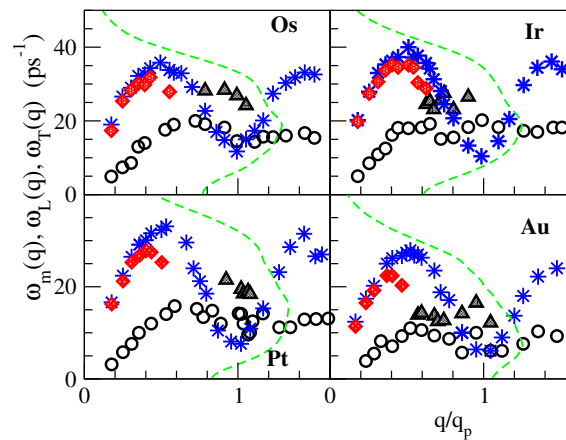

Figure 13. (Colour online) Same as the previous graph, but for l-Os, l-Ir, l-Pt and l-Au.

The $C_T(q, t)$ has a mathematical structure which evolves from a gaussian function, in both q and t, at the free particle ($q \rightarrow \infty$) limit, towards a gaussian in q and exponential in t at the hydrodynamic limit ($q \rightarrow 0$). Although in both limits, the $C_T(q, t)$ is always positive, for intermediate q-values it generally displays noticeable oscillations around zero [38, 45–47], related to the propagation of damped shear waves.

Its associated spectrum $C_T(q, \omega)$, when plotted as a function of ω, shows within some q-range, clear peaks which indicate the frequencies of the propagating shear waves. In the present AIMD simulations, the lowest attainable q value, q_{min}, is already outside the hydrodynamic region and the associated $C_T(q = q_{min}, \omega)$ displays a peak which attests to the propagation of shear waves. With increasing q-values, we obtain that the frequency of the peak, $\omega_T(q)$, increases, reaches a maximum at $q \approx (2/3) q_p$,
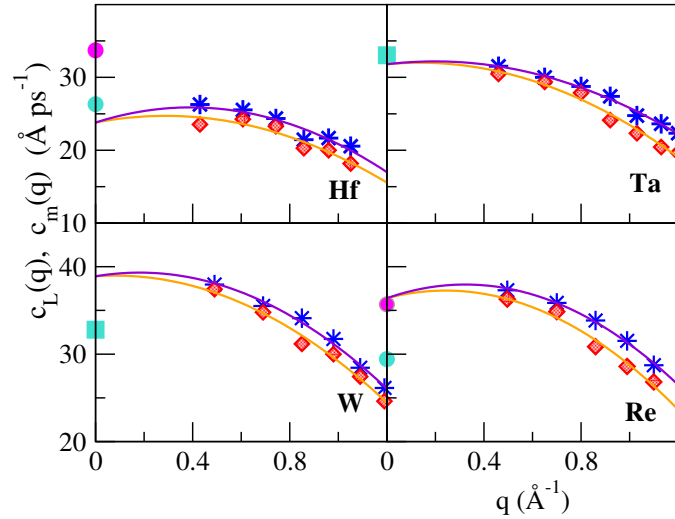
Figure 14. (Colour online) Phase velocities as obtained from maxima in $S(q, \omega)$ (red diamonds) and from $C_L(q, \omega)$ (blue stars) for l-Hf, l-Ta, l-W and l-Re. Lines are fits using a quadratic formula to both datasets with a common value at $q = 0$. Magenta circles denote estimations for the adiabatic sound velocities, c_s, from [5]. Turquoise circles are estimations for c_s from [4] and turquoise squares are measured values of c_s as reported in [4].
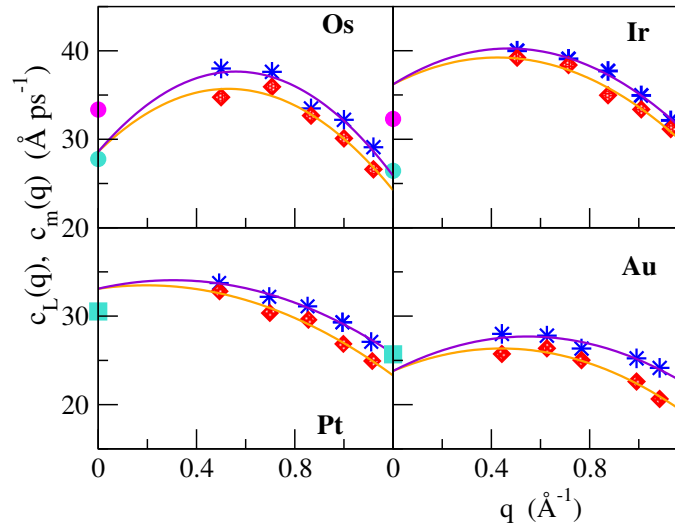

Figure 15. (Colour online) Same as the previous figure, but for l-Os, l-Ir, l-Pt and l-Au.

and after a slight initial decrease, the $\omega_T(q)$ remains practically constant until $q \approx 3.0 \, q_p$ when the peaks disappear. Furthermore, we also find, for some metals, another peak with a higher frequency, although its appearance lasts over a much smaller q-range located around the position of the main peak of $S(q)$. These features are depicted in figures 12–13 where we plotted the high and low-frequency dispersion relations for the transverse modes. Notice that the two branches occur in all of the systems except l-Hf.

A few years ago, Bryk et al. [48] reported for the first time the presence of such a second, high-frequency, transverse branch in an AIMD study of l-Li at high pressures, and this result was later confirmed by similar findings in AIMD calculations of high pressure l-Na and l-Fe [49, 50]. Although it was initially considered to be a feature induced by the high pressure state, subsequent studies revealed a second high-frequency transverse branch in AIMD studies of l-Tl, l-Pb, l-Zn, l-Sn, and some liquid $3d$ and $4d$ transition metals at ambient pressure [30–32, 42, 51–54]. A possible explanation for the appearance

of this second transverse branch was put forward in terms of mode-coupling (MC) ideas [53, 54].

Recently, Bryk and coworkers [42, 51, 52] pointed out to the simultaneous appearance of both the high frequency transverse modes and the presence of another, high frequency peak/shoulder, in the spectra of the VACF, namely $Z(\omega)$. They observed this feature in AIMD studies of l-Tl and l-Pb; moreover, they found a definite correlation between the frequency peaks of the $Z(\omega)$ and the average frequencies, in the q region between $q_p/2$ and q_p, of both high- and low frequency transverse branches. The present AIMD simulation results ratify this connection between the structure of the $Z(\omega)$ and the existence of one/two transverse dispersion branches. According to figures 12–13, we find that l-Hf has a $Z(\omega)$ with one peak and the associated transverse dispersion relation displays just one, low-frequency, branch. However, for the other $5d$ metals we observe that the associated $Z(\omega)$ displays one peak along with a (higher-frequency) shoulder/peak and the corresponding transverse dispersion shows two branches. We note that a similar correspondence was found in AIMD simulation studies of several liquid $3d$ and $4d$ transition metals [30–32]. In principle, such a connection should not be unexpected because several years ago Gaskell and Miller [55–57] used the MC theory to formulate a theory of the VACF based on contributions arising from the coupling of the single particle motion to the collective longitudinal and transverse currents. However, a more detailed account about the way these correlations are established is still lacking.

From the AIMD results for the $C_T(q,t)$, we also evaluated [45, 46, 58, 59] the associated shear viscosity coefficient, η, and in table 4 we report our results along with the available experimental data. Fortunately, despite the technical challenges caused by these $5d$ refractory metals, their respective viscosities were measured by means of levitation techniques [5–8] with an uncertainty of around 10%. We obtain a fair agreement with experimental data even though we observe, for some metals, noticeable differences among those data.
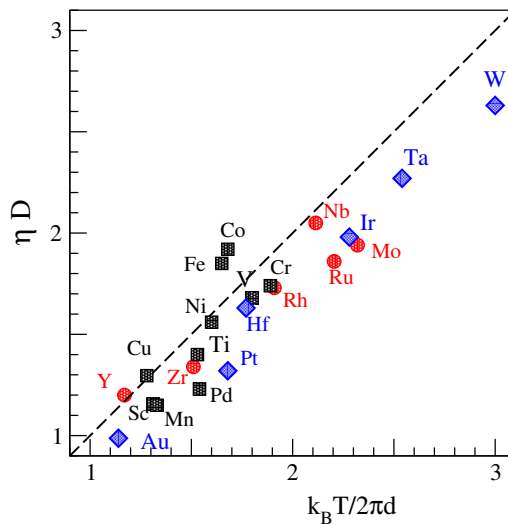

Figure 16. (Colour online) Stokes-Einstein relation. Black squares: $3d$ metals. Red circles: $4d$ metals. Blue diamonds: $5d$ metals.

The study of transport properties in metallic liquids has often resorted to the Stokes-Einstein (SE) relation which establishes a connection between the self-diffusion coefficient D of a particle with a diameter d moving in a liquid of viscosity η. Although the SE relation was originally aimed at brownian particles and, therefore, was derived by using purely macroscopic considerations, it was found to work rather well for many monoatomic liquids [47]. In the slip condition, the SE relation reads as $\eta D = k_B T/2\pi d$ and it has often been used to estimate η (or D) by identifying d with the position of the main peak of $g(r)$. In the specific case of MD simulations, as the evaluation of the self-diffusion coefficient takes much less computation time than the calculation of the shear viscosity, then it has become a common practice to use the SE relation to get an estimate of the shear viscosity. Moreover, the SE relation has also been used in the derivation of several semiempirical formulae connecting, in terms of

other thermophysical magnitudes, the shear viscosity and the self-diffusion coefficient.

By using the present AIMD results for the diffusion coefficients and the viscosities of the liquid $5d$ metals we have analyzed the accuracy of the SE relation. The results are plotted in figure 16, along with similar AIMD-based data for the liquid $3d$ and $4d$ metals [30–32].
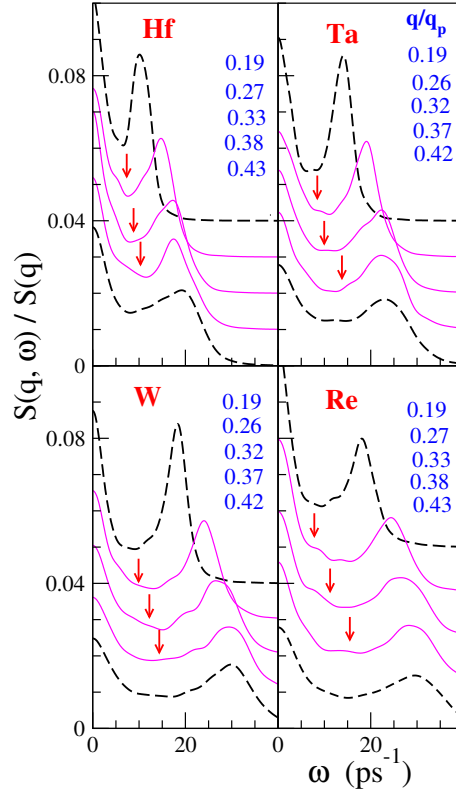

Figure 17. (Colour online) AIMD calculated dynamic structure factors $S(q,\omega)/S(q)$ for l-Hf, l-Ta, l-W and l-Re at various (top to bottom) q/q_P values. The vertical scales are offset for clarity. The arrows point to the locations of the maxima in the $C_T(q,\omega)$.

In the last few years, another topic of interest has been the appearance of small, weak shoulders in the dynamic structure factor of liquid metals at wavevectors in the wavevector region around $q_p/2$ and the frequency region between the quasielastic and inleastic peaks. These features were first noticed in an IXS measurement of the $S(q,\omega)$ of l-Ga near melting [60] and were corroborated by an OF-AIMD simulation study. They were interpreted as transverse-like low-energy excitations and were also found in both measurements and AIMD simulation studies [28–32, 61, 62] for a range of liquid metals.

Figures 17–18 show our AIMD simulation results for $S(q,\omega)$ at several q-values below $q_p/2$. We established that for most of these liquid metals (except l-Pt and l-Au), the corresponding $S(q,\omega)$ shows the appearance of some weak shoulders whose energies are close to those corresponding to the (low-frequency) peaks in the transverse current spectra. The physical origin of these low energy excitations in liquid metals is still a moot point because no sound theoretical scheme has provided an explanation as to how transverse currents could couple to longitudinal excitations. Other possible interpretations, such as relaxing (non-propagating) terms or non-lorentzian (asymmetry) terms [63, 64], or as kinetic heat waves [65] have also been proposed.

3.3. Electronic properties: density of states

We also calculated the partial and total electronic density of states, $n(E)$. This was obtained from the self-consistently determined eigenvalues, averaged over four ionic configurations well separated in time (≈ 15.0 ps), sampling the Brillouin zone with a mesh of $2 \times 2 \times 2$ points.
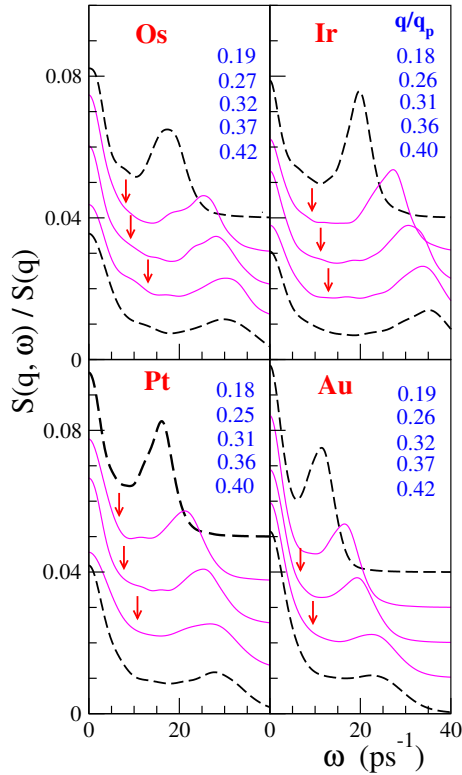
Figure 18. (Colour online) Same as the previous graph, but for for l-Os, l-Ir, l-Pt and l-Au.
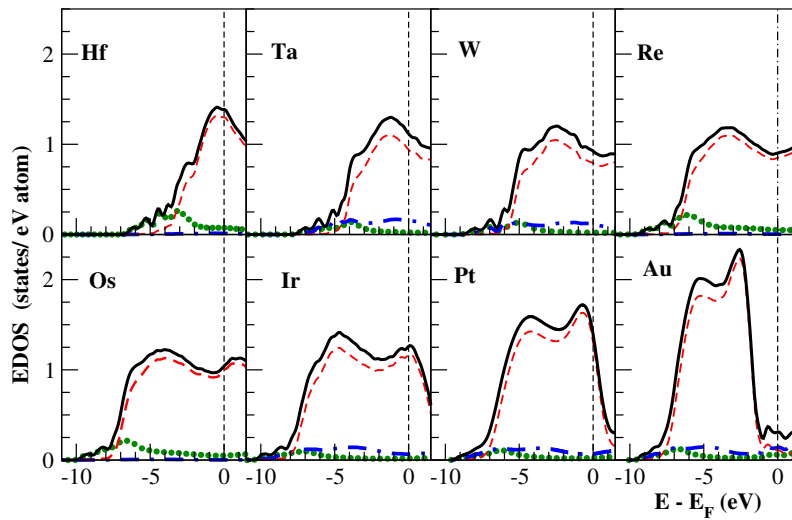

Figure 19. (Colour online) Total electronic density of states (black line) for several $5d$ transition metals. The angular momentum decomposition of the DOS in s (green dotted line), p (blue dashed-dotted line) and d (red dashed line). Data for l-Pt are taken from [17].

Figure 19 shows the obtained results for the electronic partial and total $n(E)$ associated to the outer valence electrons. The $n(E)$ is dominated by the $5d$ states which are progressively filled with increasing atomic number. This is reflected in the increase of the height and/or width of the $n(E)$ as the occupation rises. Additional (and smaller) contributions from the $6p$ and $6s$ states are also observed.

The integrated partial densities of states up to the Fermi level indicate the ocupations of the corre-

sponding s, p and d bands. Such ocupations are not integer in general, and add up to the total number of valence electrons per atom. Neglecting the lower lying $5s$ and $5p$ atomic states, the occupations of the bands are reported in table 5. These data may be of value for some models that treat within different approximate schemes the s, p electrons and the d electrons in order to obtain effective interatomic pair potentials [66–68].

Table 5. Occupations of the s, p and d bands in the liquid $5d$ metals considered.

	Hf	Ta	W	Re	Os	Ir	Pt	Au
$6s$	0.8	0.3	0.3	1.0	1.0	0.4	0.4	0.5
$6p$	0.0	0.8	0.9	0.0	0.0	1.0	0.9	1.0
$5d$	3.2	3.9	4.8	6.0	7.0	7.6	8.7	9.5
sp	0.8	1.1	1.2	1.0	1.0	1.4	1.3	1.5

4. Conclusions

A range of static, dynamic and electronic properties of several liquid $5d$ transition metals have been calculated by using an *ab initio* simulation method. Although there were some previous studies for l-Ta and l-Au, this is the first comprehensive AIMD study performed on their liquid state properties near melting, except l-Pt, whose results are also included here for completion.

As for the static structure, we obtain a good agreement with the available experimental data in those two metals (l-Pt and l-Au) for which the comparison can be performed. The calculated $S(q)$ displays an asymmetric shape in its second peak with a marked shoulder in l-Hf, l-Ta, l-W and l-Re. This feature is connected with the existence icosahedral short-range order in the liquid. A subsequent analysis based on the CNA method shows that these four metals have the greatest abundance of five-fold type structures.

The AIMD dynamic structure factors, $S(q, \omega)$, show side-peaks which are indicative of collective density excitations. Furthermore, we have also found that the $S(q, \omega)$ associated to most of these metals (except l-Pt and l-Au) exhibit, within some q-range, some kind of excitations which have the features similar to the transverse-like excitation modes found in IXS and INS experimental data for several other liquid metals.

The AIMD transverse current correlation functions, $C_T(q, t)$, display oscillations around zero, while their spectra, $C_T(q, \omega)$, show peaks which point to the existence of shear waves. Except l-Hf, we have found that the respective transverse dispersion relations exhibit two branches. These results support the proposed connection between the structure of the spectra of the VACF and the existence of one/two transverse dispersion branches.

From the previous time correlation functions, we have also evaluated some transport coefficients, namely the self-diffusion, adiabatic sound velocity and shear viscosity coefficients. Taking into account the scarcity of data concerning most of these coefficients we expect that the present results will be helpful. Finally, the previous results for self-diffusion and shear viscosity have been used to analyze the accuracy of the Stokes-Einstein relationship for these liquid metals.

Acknowledgements

References

1. Waseda Y., The Structure of Non-Crystalline Materials, McGraw-Hill, New York, 1980.

2. Katagiri K., Ozaki N., Ohmura S., Albertazzi B., Hironaka Y., Inubushi Y., Ishida K., Koenig M., Miyanishi K., Nakamura H., et al., Phys. Rev. Lett., 2021, **126**, 175503, doi:10.1103/PhysRevLett.126.175503.

3. Guarini E., Bafile U., Barocchi F., de Francesco A., Farhi E., Formisano F., Laloni A., Orecchini A., Polidori A., Puglini M., Sacchetti F., Phys. Rev. B, 2013, **88**, 104201, doi:10.1103/PhysRevB.88.104201.

4. Blairs S., Int. Mater. Rev., 2007, **52**, 321, doi:10.1179/174328007X212490.

5. Iida T., Guthrie R. I. L., The Thermophysical Properties of Metallic Liquids, Oxford University Press, Oxford, 2015.

6. Ishikawa T., Paradis P. F., Itami T., Yoda S., J. Chem. Phys., 2003, **118**, 7912, doi:10.1063/1.1564050.

7. Ishikawa T., Paradis P. F., Okada J. T., Watanabe Y., Meas. Sci. Technol., 2012, **23**, 025305, doi:10.1088/0957-0233/23/2/025305.

8. Ishikawa T., Paradis P. F., Okada J. T., Kumar M. V., Watanabe Y., J. Chem. Thermodyn., 2013, **65**, 1, doi:10.1016/j.jct.2013.05.036.

9. Alemany M. M. G., Rey C., Gallego L. J., J. Chem. Phys., 1998, **109**, 5175, doi:10.1063/1.477133.

10. Alemany M. M. G., Diéguez O., Rey C., Gallego L. J., Phys. Rev. B, 1999, **60**, 9208, doi:10.1103/PhysRevB.60.9208.

11. Gosh R. C., Amin M. R., Bhuiyan G. M., J. Mol. Liq., 2013, **188**, 148, doi:10.1016/j.molliq.2013.09.034.

12. Bhuiyan G. M., Gonzalez L. E., Gonzalez D. J., Condens. Matter Phys., 2012, **15**, 33604, doi:10.5488/CMP.15.33604.

13. Hohenberg P., Kohn W., Phys. Rev., 1964, **136**, B864, doi:10.1103/PhysRev.136.B864.

14. Kohn W., Sham L. J., Phys. Rev., 1965, **140**, A1133, doi:10.1103/PhysRev.140.A1133.

15. Jakse N., Le Bacq O., Pasturel A., Phys. Rev. B, 2004, **70**, 174203, doi:10.1103/PhysRevB.70.174203.

16. Jakse N., Le Bacq O., Pasturel A., J. Non-Cryst. Solids, 2007, **353**, 3684, doi:10.1016/j.jnoncrysol.2007.05.131.

17. del Rio B. G., González L. E., González D. J., Modell. Simul. Mater. Sci. Eng., 2020, **28**, 045002, doi:10.1088/1361-651X/ab7e38.

18. Giannozzi P., Baroni S., Bonini N., Calandra M., Car R., Cavazzoni C., Ceresoli D., Chiarotti G. L., Cococcioni M., Dabo I., et al., J. Phys.: Condens. Matter, 2009, **21**, 395502, doi:10.1088/0953-8984/21/39/395502.

19. Giannozzi P., Andreussi O., Brumme T., Bunau O., Buongiorno Nardelli M., Calandra M., Car R., Cavazzoni C., Ceresoli D., Cococcioni M., et al., J. Phys.: Condens. Matter, 2017, **29**, 465901, doi:10.1088/1361-648X/aa8f79.

20. Perdew J. P., Burke K., Ernzerhof M., Phys. Rev. Lett., 1996, **77**, 3865, doi:10.1103/PhysRevLett.77.3865.

21. Perdew J. P., Zunger A., Phys. Rev. B, 1981, **23**, 5048, doi:10.1103/PhysRevB.23.5048.

22. Vanderbilt D., Phys. Rev. B, 1990, **41**, 7892, doi:10.1103/PhysRevB.41.7892.

23. Calderín L., González D. J., González L. E., López J. M., J. Chem. Phys., 2008, **129**, 194506, doi:10.1063/1.3020304.

24. Calderín L., González L. E., González D. J., J. Chem. Phys., 2009, **130**, 194505, doi:/10.1063/1.3137582.

25. Calderín L., González L. E., González D. J., J. Phys.: Condens. Matter, 2011, **23**, 375105, doi:10.1088/0953-8984/23/37/375105.

26. Calderín L., González L. E., González D. J., J. Phys.: Condens. Matter, 2013, **25**, 065102, doi:10.1088/0953-8984/25/6/065102.

27. del Rio B. G., González D. J., González L. E., Phys. Fluids, 2016, **28**, 107105, doi:10.1063/1.4966656.

28. del Rio B. G., González L. E., González D. J., J. Chem. Phys., 2017, **146**, 034501, doi:10.1063/1.4973803.

29. del Rio B. G., Rodriguez O., González L. E., González D. J., Comput. Mater. Sci, 2017, **139**, 243, doi:10.1016/j.commatsci.2017.07.027.

30. del Rio B.G., Pascual C., Rodriguez O., González L.E., González D.J., Condens. Matter Phys., 2020, **23**, 23606, doi:10.5488/CMP.23.23606 .

31. del Rio B. G., González L. E., González D. J., J. Phys.: Condens. Matter, 2020, **32**, 214005, doi:10.1088/1361-648X/ab6f16.

32. González L. E., González D. J., Int. J. Refract. Met. Hard Mater., 2022, **107**, 105898, doi:10.1016/j.ijrmhm.2022.105898.

33. Waseda Y., Ohtani M., Phys. Stat. Sol. B, 1974, **62**, 535, doi:10.1002/pssb.2220620224.

34. Schenk T., Holland-Moritz D., Simonet V., Bellissent R., Herlach D. M., Phys. Rev. Lett., 2002, **89**, 075507, doi:10.1103/PhysRevLett.89.075507.

35. Lee G. W., Gangopadhyay A. K., Kelton K. F., Hyers R. W., Rathz T. J., Rogers J. R., Robinson D. S., Phys. Rev. Lett., 2004, **93**, 037802, doi:10.1103/PhysRevLett.93.037802.

36. Lee G. W., Gangopadhyay A. K., Hyers R. W., Rathz T. J., Rogers J. R., Robinson D. S., Goldman A. I., Kelton K. F., Phys. Rev. B, 2008, **77**, 184102, doi:10.1103/PhysRevB.77.184102.

37. Marcus Y., J. Chem. Thermodyn., 2017, **109**, 11, doi:10.1016/j.jct.2016.07.027.

38. Balucani U., Zoppi M., Dynamics of the Liquid State, Clarendon, Oxford, 1994.

39. Honeycutt J. D., Andersen H. C., J. Phys. Chem., 1987, **91**, 4950, doi:10.1021/j100303a014.

40. Clarke A. S., Jonsson H., Phys. Rev. E, 1993, **47**, 3975, doi:10.1103/PhysRevE.47.3975.
41. Luo W. K., Sheng H. W., Alamgir F. M., Bai J. M., He J. H., Ma E., Phys. Rev. Lett., 2004, **92**, 145502, doi:10.1103/PhysRevLett.92.145502.
42. Bryk T., Demchuk T., Jakse N., Wax J. F., Front. Phys., 2018, **6**, 00006, doi:10.3389/fphy.2018.00006.
43. Scopigno T., Ruocco G., Sette F., Rev. Mod. Phys., 2005, **77**, 881, doi:10.1103/RevModPhys.77.881.
44. Bryk T., Mryglod I., Scopigno T., Ruocco G., Gorelli F., Santoro M., J. Chem. Phys., 2010, **133**, 024502, doi:10.1063/1.3442412.
45. González D. J., González L. E., López J. M., Stott M. J., J. Chem. Phys., 2001, **115**, 2373, doi:10.1063/1.1389473·
46. González D. J., González L. E., López J. M., Stott M. J., Phys. Rev. B, 2002, **65**, 184201, doi:10.1103/PhysRevB.65.184201.
47. Hansen J. P., McDonald I. R., Theory of Simple Liquids, Academic Press, London, 1986.
48. Bryk T., Ruocco G., Scopigno T., Seitsonen A. P., J. Chem. Phys., 2015, **143**, 104502, doi:10.1063/1.4928976.
49. Marqués M., González L. E., González D. J., Phys. Rev. B, 2015, **92**, 134203, doi:10.1103/PhysRevB.92.134203.
50. Marqués M., González L. E., González D. J., J. Phys.: Condens. Matter, 2016, **28**, 075101, doi:10.1088/0953-8984/28/7/075101.
51. Bryk T., Demchuk T., Jakse N., Phys. Rev. B, 2019, **99**, 014201, doi:10.1103/PhysRevB.99.014201.
52. Bryk T., Jakse N., J. Chem. Phys., 2019, **151**, 034506, doi:10.1063/1.5099099.
53. del Rio B. G., González L. E., Phys. Rev. B, 2017, **95**, 224201, doi:10.1103/PhysRevB.95.224201.
54. del Rio B. G., Chen M., González L. E., Carter E. A., J. Chem. Phys., 2018, **149**, 094504, doi:10.1063/1.5040697.
55. Gaskell T., Miller S., J. Phys. C: Solid State Phys., 1978, **11**, 3749, doi:10.1088/0022-3719/11/18/012.
56. Gaskell T., Miller S., J. Phys. C: Solid State Phys., 1978, **11**, 4839, doi:10.1088/0022-3719/11/24/015.
57. Gaskell T., Miller S., Phys. Lett. A, 1978, **66**, 307, doi:10.1016/0375-9601(78)90246-3.
58. Palmer B. J., Phys. Rev. E, 1994, **49**, 359, doi:10.1103/PhysRevE.49.359.
59. Balucani U., Brodholt J. P., Jedlovszky P., Vallauri R., Phys. Rev. E, 2000, **62**, 2971, doi:10.1103/PhysRevE.62.2971.
60. Hosokawa S., Inui M., Kajihara Y., Matsuda K., Ichitsubo T., Pilgrim W. C., Sinn H., González L. E., González D. J., Tsutsui S., Baron A. Q. R., Phys. Rev. Lett., 2009, **102**, 105502, doi:10.1103/PhysRevLett.102.105502.
61. Hosokawa S., Munejiri S., Inui M., Kajihara Y., Pilgrim W. C., Ohmasa Y., Sutsui T., Baron A. Q. R., Shimojo F., Hoshino K., J. Phys.: Condens. Matter, 2013, **25**, 112101, doi:10.1088/0953-8984/25/11/112101.
62. Hosokawa S., Munejiri S., Inui M., Kajihara Y., Pilgrim W. C., Baron A. Q. R., Shimojo F., Hoshino K., AIP Conf. Proc., 2013, **1518**, 695, doi:10.1063/1.4794661.
63. Montfrooij W., Bafile U., Guarini E., Phys. Fluids, 2021, **33**, 087114, doi:10.1063/5.0057076.
64. Ishikawa D., Baron A. Q. R., J. Phys. Soc. Jpn., 2021, **90**, 083602, doi:10.7566/JPSJ.90.083602.
65. Bryk T., Wax J. F., J. Chem. Phys., 2016, **144**, 194501, doi:10.1063/1.4948709.
66. Wills J. M., Harrison W. A., Phys. Rev. B, 1983, **28**, 4363, doi:10.1103/PhysRevB.28.4363.
67. Dubinin N. E., J. Phys.: Conf. Ser., 2012, **338**, 012004, doi:10.1088/1742-6596/338/1/012004.
68. Dubinin N. E., Bhuiyan G. M., Abbas F. I., Russ. Metall., 2019, **2019**, 835, doi:10.1134/S0036029519080044.

Першопринципні дослідження статичних, динамічних та електронних властивостей деяких рідких 5d перехідних металів поблизу точок плавлення

Д. Х. Гонзалес, Л. Е. Гонзалес

Факультет теоретичної фізики, Університет Вальядоліду, 47011 Вальядолід, Іспанія

Представлено результати дослідження статичних та динамічних властивостей низки рідких $5d$ перехідних металів в термодинамічних умовах в околі відповідних точок плавлення. Дослідження проведено шляхом першопринципного моделювання методом молекулярної динаміки в рамках теорії функціоналу густини. Представлено результати для статичних структурних факторів і парних функцій розподілу; також аналізується локальний ближній порядок в рідких металах. Обчислено як одночастинкові, так і колективні динамічні характеристики. Отримана динамічна структура свідчить про флуктуації густини. Також отримано відповідне дисперсійне співвідношення і низку результатів для поздовжних і поперечних спектральних функцій струмів разом з пов'язаною з ними дисперсією колективних збуджень. Для деяких металів виявлено існування двох гілок поперечних колективних збуджень в області поблизу головного піку структурного фактора. Проведено розрахунок деяких коефіцієнтів переносу.

Ключові слова: *рідкі метали, перехідні метали, першопринципні розрахунки*